Electronic Supplementary Information

Contact loss and its improvement at interface between cathode and solid electrolyte in all solid-state battery based on the multi-scale & multi-physics analysis

Taesoon Hwang,[ab] Ingyun Chung,[bc] Sunyoung Im,[bc] Jonggeon Lee,[b] Maenghyo Cho[b] and Kyeongjae Cho[a]

[a] *Department of Materials Science and Engineering, University of Texas at Dallas, Richardson, TX 75080, USA. E-mail: kjcho@utdallas.edu.*

[b] *Department of Mechanical and Aerospace Engineering, Seoul National University, 1 Gwanak-ro, Gwanak-gu, Seoul 08826, Republic of Korea.*

[c] *Samsung electronics,1, Samsung-ro, Giheung-gu, Yongin-si, Gyeonggi-do, Republic of Korea.*

Methods

First-principles calculation

The atomic and electronic structures of NCM811 and LGPS were examined by the density functional theory(DFT). The DFT calculations were conducted by using the Vienna Ab Initio Simulation Package (VASP) with the exchange-correlation functional of spin-polarized generalized gradient approximation (GGA) parameterized by Perdew-Burke-Ernzerhof (PBE).[51,52] In the simulation of the NCM811, the bulk structures consist of 2×2×1 unit cells and k-point of Monkhorst-Pack grid 4×4×2 was applied, while the surface models of the (104) plane are calculated based on k-point of Gamma centered grid 1×2×1 with a total of 20 Å vacuum slabs. The Hubbard U correction was applied to mitigate the strong correlation of TM's 3d electron bands in the both bulk and surface calculations. The following U values are 5.2 eV for Mn, 5.9 eV for Co and 6.8 eV for Ni based on previous study.[47] In additions, in the simulation of the LGSP, the bulk structures consist of 1×1×1 unit cells and k-point of Monkhorst-Pack grid 4×4×2 was applied, while the surface models of the (101) plane are calculated based on k-point of Gamma centered grid 2×4×1 with a total of 20 Å vacuum slabs. The cut-off energy of 500 eV was applied to the both NCM811 and LGPS calculations. In these calculations, all of the calculated structures were thermodynamically relaxed.

Molecular dynamics (MD) calculation

To calculate the material properties of polyamide and PDMS Fillers, the molecular monomer structures were first built. The polymers of polyamide and PDMS Fillers consist of 19011 and 10040 atoms and are constructed by assembling the chains consisting of respective monomers. These molecular modeling and energy relaxation were conducted by the molecular dynamics simulation software of Materials Studio 5.5 with the polymer-consistent force field (PCFF).[53] Based on the molecular models, detailed energy minimization and uniaxial tensile loading simulation were conducted for the models of polyamide and PDMS Fillers by Large-Scale Atomic/Molecular Massively Parallel Simulation (LAMMPS). For the energy minimization for the two materials, the MD simulation was followed successively by energy minimization, canonical ensemble(NVT) at 500 K for 3 ns, NVT at 300 K for 4 ns and isothermal-isobaric ensemble(NPT) at 300 K under atmospheric pressure for 5 ns. The calculated densities of polyamide and PDMS models are 1.06 g/cm3 and 0.94 g/cm3, which are well consistent with the experimental values of each material.[54,55] Based on the stably relaxed model, we calculated the material properties.

Finite element method simulation

To analyze the mechanism of contact loss at the interface, we designed multi-scale & multi-physics model. Especially in the proposed models, the micro/macro scale part was organized with two part

electrochemical models and mechanical models. The proposed electro-chemo-mechanical multi-scale & multi-physics model described in detail next was solved by FEM. The electrochemical model is driven by input current flow (I) and then Li flows (Δc_{Li}) by the electrochemical model's reaction during charge used in conventional ASB system. [56-59] The cathode and SE were considered NCM811 and LGPS in the following equations. Here, we also introduced counter electrode Li metal as anode material. During the charging process, Li-ions flow to the interface and then cross the interface by charge transfer reaction in the cathode material. Subsequently, Li ions continuously flow from SE to anode material and are deposited at anode material. In the cathode material, we assume that the migration effect is negligible due to the screening effect by moving electrons. From the assumption, the flux (J_{Li^+}) of Li-ion depending on time (t) and distance (x) from the current collector in the cathode material may be described based on Fick's law as given below:

$$J_{Li^+}(x,t) = D_{Li^+}\nabla c_{Li^+} \quad \text{(S.1)}$$

$$J_{Li^+}(L_1,t) = \frac{I_{Cathode}(t)}{FA} \quad \text{(S.2)}$$

$$J_{Li^+}(0,t) = 0 \quad \text{(S.3)}$$

where $I_{Cathode}$ is reaction current of Cathode, F is Faraday's constant and A is reaction area. Here, D_{Li^+}= 3.04×10^{-13}m^2/s is considered the diffusion coefficient of NCM811 based on the reported paper. [60,61] The Li-ion flux is coupled to charge transfer reaction at the interface between cathode and SE. In the interface, electrochemical reactions occur at as given below:

$$LiNi_{0.8}Co_{0.1}Mn_{0.1}O_2 \rightleftharpoons Ni_{0.8}Co_{0.1}Mn_{0.1}O_2 + Li^+ + e^- \quad \text{(S.4)}$$

The electrochemical reaction is described by Butler-Volmer equation as given below:

$$I_{Cathode} = I^0_{Cathode}(e^{\alpha_{Cathode}(F/RT)\eta} - e^{-(1-\alpha_{Cathode})(F/RT)\eta} \quad \text{(S.5)}$$

$$I^0_{Cathode} = FAk_{Cathode}\left(\bar{a}_{Ni_{0.8}Co_{0.1}Mn_{0.1}O_2}\bar{a}_{Li^+}\right)^{\alpha_{Cathode}} \times \left(\bar{a}_{LiNi_{0.8}Co_{0.1}Mn_{0.1}O_2}\right)^{1-\alpha_{Cathode}} \quad \text{(S.6)}$$

where R is a gas constant $\bar{a}_k$ and α_k are average activity and charge transfer coefficient of species k respectively, $k_{Cathode}$= 5.1×10^{-4}m^2/s is introduced as the rate constant for the equation (S.6).[62] In these equations, η is an overpotential and may be described as given below:

$$\eta = \phi_{OV} - E_{eq} \quad \text{(S.7)}$$

$$\eta = \phi_{Cath} - \phi_{SE} - E_{eq} \quad \text{(S.8)}$$

$$= \eta_{ch} + \eta_{Cath} + \eta_{SE} \quad \text{(S.9)}$$

where ϕ_{OV} is operating voltage, E_{eq} is equivalent potential calculated in the previous chapter, ϕ_{Cath} and ϕ_{SE} are electrostatic potential of the cathode and SE, η_{ch} is charge transfer overpotential, η_{Cath} and η_{SE} are ionic diffusions in the cathode and SE materials.

Here, we assumed the possible path of Li-ion migration along *c*-axis in LGPS and then considered δ=0.7 as a mobile fraction of the total contents of Li-ion. Based on the mobile fraction, the equilibrium reaction may be described as given below:

$$Li_{10}GeP_2S_{12} \underset{k_r}{\overset{k_d}{\rightleftarrows}} Li_{10-\delta}GeP_2S_{12} + \delta Li^+ + \delta e^- \quad \text{(S.10)}$$

$$k_d = \frac{k_r a_0 \delta^2}{(1-\delta)} \quad \text{(S.11)}$$

where k_d and k_r are reaction rates of Li-ion generation and recombination. k_r= 0.9×10^{-8}m^3/s is adopted based on the reported thiophosphate solid electrolytes.[59] For these reasons, the charges in SE flow by Nernst-Plank equation as given below:

$$J_k(x,t) = -D_k \nabla c_k + \frac{z_k F}{RT} D_k c_k \nabla \phi_{SE} \quad \text{(S.12)}$$

where k is the charge species(Li$^+$ and e$^-$) and z_k is the valence for each charge species. In addition, D_{Li^+} = 2.2×10^{-12} m^2/s is the diffusion coefficient of LGPS based on the reported paper.[62] the conductivity of e$^-$ (D_{e^-}) is also applied from the reported thiophosphate solid electrolytes.[60] The fluxes driven by diffusion and migration for each charge carrier based on equation (S.12) are constraint by the boundary conditions as given below:

$$J_{Li^+}(L_1,t) = -\frac{I_{Cathode}(t)}{z_{Li^+}FA} \quad \text{(S.13)}$$

$$J_{Li^+}(L_1+L_2,t) = -\frac{I_{Anode}(t)}{z_{Li^+}FA} \quad \text{(S.14)}$$

$$J_{e^-}(L_1,t) = J_{e^-}(L_1+L_2,t) = 0 \quad \text{(S.15)}$$

where the interfaces are considered electronic insulation as described in equation (S.13). In the interface between the anode and the SE, the charge transfer reactions may be derived in the similar manner with equation (S.15) as given below:

$$Li \rightleftharpoons Li^+ + e^- \quad \text{(S.16)}$$

The electrochemical reaction is also combined and described by Butler-Volmer equation as given below:

$$I_{Anode} = I^0_{Anode}(e^{\alpha_{Anode}(F/RT)\eta} - e^{-(1-\alpha_{Anode})(F/RT)\eta} \quad \text{(S.17)}$$

$$I^0_{Anode} = FAk_{Anode}(\bar{a}_{Li^+})^{\alpha_{Anode}} \times (\bar{a}_{Li})^{1-\alpha_{Anode}} \quad \text{(S.18)}$$

where k_{Anode} =1 × 10^{-2} m^2/s is adopt as the rate constant for the equation (S.18).[60] The notations described in the electrochemical equations are all listed in Table. S1

The mechanical reactions of this interface model progressed with flux of Li concentrations fields (c_{Li^+}) that originated from electrochemical model at the same time per each iteration upon the charge. Although the electrochemical reactions of Li transference in this interface model are a dynamical time-dependent process, the mechanical equilibrium is considered an almost instantaneous process due to especially fast strain variations in elastic media that the cathode material is contracted during the charging process. For

these reasons, a quasi-static process is introduced to analyze this mechanical model at every iteration during the charge.[62]

In the mechanical model, we adopted the electrochemical strain based on the calculated volume depending on Li concentration changes by assuming that the cathode material indicates continuous contraction during the charging process as given below:

$$\varepsilon_{el} = \varepsilon(\mathrm{c_{Li^+}}) = \frac{1}{3}\left(\frac{V\mathrm{c_{Li^+}} - V_0}{V_0}\right)\Delta\mathrm{c_{Li^+}} \qquad \text{(S.19)}$$

where ε is a strain, $V\mathrm{c_{Li^+}}$ is volume according to concentration and V_0 initial volume. The electrochemical strain was applied to the following mechanical fracture model.[62]

To examine the contact loss that is the crack initiation and propagation at the interface during the charge, we adopt the phase field approximation of crack topology based on the introduced reports.[63-65] Here, crack is represented as auxiliary field variable $\mathrm{d} \in [0,1]$ where d=0 is unbroken state and d=1 is fully broken state in the interface model. By using the crack variable, the crack surface density function is introduced as given below:

$$\gamma(d, \nabla d) = \frac{1}{2l}d^2 + \frac{1}{2}|\nabla d|^2 \qquad \text{(S.20)}$$

In addition, the crack surface density is assumed that the degradation originated from only the tension. Therefore, the strain energy density is decomposed into tensile and compressive parts:

$$\psi = \psi^+ + \psi^- \qquad \text{(S.21)}$$

$$\psi^+ = \frac{1}{2}\lambda\langle tr(\varepsilon)\rangle_+^2 + \mu tr(\varepsilon_+^2) \qquad \text{(S.22)}$$

$$\psi^- = \frac{1}{2}\lambda\langle tr(\varepsilon)\rangle_-^2 + \mu tr(\varepsilon_-^2) \qquad \text{(S.23)}$$

where λ and$\mu$are the Lamé constants, ε_+ and ε_+ are the tensile and compressive part, the brackets are as given below:

$$\varepsilon_+ = \sum_{i=1}\langle\varepsilon^i\rangle_+ + \mathrm{n}^i \otimes \mathrm{n}^i \qquad \text{(S.24)}$$

$$\varepsilon_- = \sum_{i=1}\langle\varepsilon^i\rangle_- + \mathrm{n}^i \otimes \mathrm{n}^i \qquad \text{(S.25)}$$

where ε^i is the principle strain, the bracket operators are $\langle x\rangle_+ = (x + |x|)/2$ and $\langle x\rangle_- = (x - |x|)/2$. From these equations, strain energy by the phase field may be introduced as given below:

$$\psi(d, \varepsilon) = [(1-d)^2 + p]\psi^+(\varepsilon) + \psi^-(\varepsilon) \qquad \text{(S.26)}$$

where p is control parameter to conserve the tensile part depending on crack filed variable. In addition, to guarantee the continuous tension, the history strain filed is introduced by replacing $\psi^+(t)$ as give below:

$$\mathcal{H} = \begin{cases} \psi^+(t) & \text{for } \psi^+(t) > \mathcal{H}(t-1) \\ \mathcal{H}(t-1) & \text{otherwise} \end{cases} \qquad \text{(S.27)}$$

The energy functional combing conventional mechanical strain energy and crack generation energy may be derived considering the fracture energy ($\mathrm{G_c}$) as given below:

$$\Pi = \frac{1}{2}\int \sigma\epsilon \, dV - \int bu \, dV - \int fu \, dS - \int G_c\gamma(d, \nabla d) \, dV \quad \text{(S.28)}$$

where the b and f are body force and surface traction respectively. Here, the elastic energy term in equation (S.28) is decomposed by equation (S.19) and (S.26) to consider electrochemical strain as given below:

$$\Pi = \frac{1}{2}\int \psi(d, \varepsilon) \, dV - \frac{1}{2}\int \mathrm{Y}{\varepsilon_{el}}^2 \, dV$$
$$- \int bu \, dV - \int fu \, dS - \int G_c\gamma(d, \nabla d) \, dV \quad \text{(S.29)}$$

By applying the variational principle for the energy functional in equation (41) and mechanical equilibrium, the governing equations are derived as given below:

$$\nabla_\epsilon \sigma - \mathrm{Y}\varepsilon_{el} = 0 \quad \text{(S.30)}$$

$$\nabla_d \left[\frac{1}{2}\psi(d, \varepsilon) + G_c\gamma(d, \nabla d)\right] = 0 \quad \text{(S.31)}$$

In the proposed model, these master equations were solved by the staggered update process that calculates successively the displacement field and crack field variables for computational convenience. This mechanical deformation progressively-generated at every iteration has an effect on the Li flow. The crack propagation at the interface blocks the flow and forces a detour of Li flux. It induces the electro chemical resistance and then change electrochemical environment again.

Hyperelastic method

To analysis on material properties of designed polymer models for polyamide and PDMS Fillers, the uniaxial tensile loading simulation is conducted to obtain stress-strain curve and then Mooney-Rivlin model is applied to the obtained stress-strain curves to calculate hyperelastic properties.[48] The uniaxial tensile loading simulations are carried out by NPT at 300 K under 1 atm with strain rates of 10^8/s until 15% strain for the polyamide and 10^9/s until 5% strain for the PDMS. On the atomic scales, the mechanical Cauchy stress is described by the virial theorem as given below:

$$\sigma^{MD} = \frac{1}{|\Omega|}\left(-\sum_{i\in\Omega} m_i v_i v_i^T + \frac{1}{2}\sum_{i\in\Omega}\sum_{j\neq i} r_{ij} F_{ij}\right) \quad \text{(S.32)}$$

where Ω is domain of the system, m_i and v_i are the mass and velocity vector of atom *I*, respectively , r_{ij} is the relative position of vector between atom *i* and *j*, F_{ij} is the interatomic force vector on atom *i* by atom *j.*[48] The biaxial tensile tests are conducted repetitively to a total of 30 simulations averaged along with x, y and z directions. The results are then averaged for accuracy.

In this study, generalized Mooney-Rivlin model is applied for the polyamide and PDMS fillers with hyperelastic properties.[48] The strain energy (W) for the hyperelastic model is described as given below:

$$W = \sum_{p=0}^{N_p}\sum_{q=0}^{N_q} C_{pq}\,(J_1 - 3)^p (J_2 - 3)^q + \frac{1}{2}\sum_{m=1}^{N_m} \kappa_m\,(J - 1)^{2m} \quad \text{(S.33)}$$

Where J_1 and J_2 are the first and second reduced invariant of the Cauchy-Green deformation tensors (C = $F^T F$), J is the jacobian of the deformation tensor (F), C_{pq} and κ_m are the inherent material coefficients, N_p, N_q and N_m are the order of polynomials. These invariants are indicated as given below:

$$J_1 = I_1 I_3^{-1/3},\ J_2 = I_2 I_3^{-2/3}\ ,J = I_1 I_3^{-1/3}$$

$$I_1 = tr(\mathrm{C}), I_1 = \frac{1}{2}\{(tr(\mathrm{C}))^2 - tr(\mathrm{C}^2)\} \text{ and } I_3 = det(\mathrm{C}) \qquad \text{(S.34)}$$

The Cauchy stress in the generalized Mooney-Rivlin model is explained as given below:

$$\sigma^{Mooney-Rivlin} = J^{-1}\mathrm{F}S\mathrm{F}^{\mathrm{T}} = J^{-1}\mathrm{F}\left(\frac{\partial W}{\partial E}\right)\mathrm{F}^{\mathrm{T}} \qquad \text{(S.35)}$$

where S is the second Piola-Kirchhoff stress and E is Green-Lagrangian strain. The derivative of W with respect to E is described as given below:

$$\frac{\partial W}{\partial E} = \frac{\partial W}{\partial J}\frac{\partial J}{\partial E} = \frac{\partial W}{\partial J_1}\frac{\partial J_1}{\partial E} + \frac{\partial W}{\partial J_2}\frac{\partial J_2}{\partial E} + \frac{\partial W}{\partial J}\frac{\partial J}{\partial E}$$

$$\frac{\partial J_1}{\partial E} = 2\mathrm{I}(I_3)^{-1/3} - \frac{2}{3}I_1(I_3)^{-1/3}(\mathrm{C})^{-1}$$

$$\frac{\partial J_2}{\partial E} = 2(I_1\mathrm{I} - \mathrm{C})(I_3)^{-1/3} - \frac{4}{3}I_2(I_3)^{-2/3}\mathrm{C}^{-1}$$

$$\frac{\partial J_3}{\partial E} = (I_3)^{-1/2}\mathrm{C}^{-1} \qquad \text{(S.36)}$$

Based on these MD and Mooney-Rivlin model, the hyperelastic material coefficients of C_{pq} and κ_m are derived by the nonlinear least square fitting method minimizing the deviation between the Cauchy stresses of MD (σ^{MD}) and Mooney-Rivlin model ($\sigma^{Mooney-Rivlin}$).[48] Here, the strain energy (W_s) for two parameter Mooney-Rivlin model of nearly incompressible state with N_p=1, N_q=1 and N_m=1 is applied to calculate the material parameters for a computational convenience as given below:

$$W_s = C_{10}(J_1 - 3) + C_{01}(J_2 - 3) + \frac{1}{2}\kappa(J-1)^2 \qquad \text{(S.37)}$$

From the equation and the nonlinear least square fitting method, the hyperelastic material properties are calculated as shown in Fig. S8 and the derived coefficients are listed in Table 2.

Supplementary data

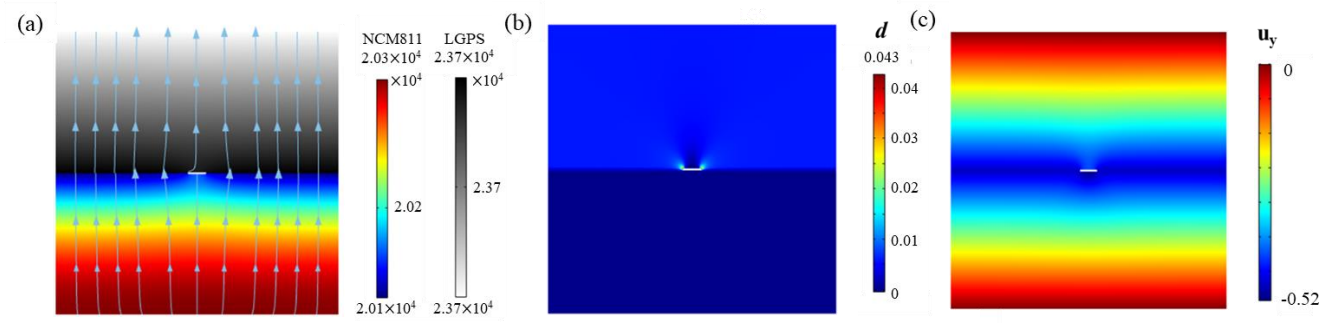

Fig. S1 Electro-chemo-mechanical responses of (a)Li concentration [mol/m^3], (b)crack field[*0*≤d≤1], (c)displacements [u_y(nm)] at 600s (SOC=0.17).

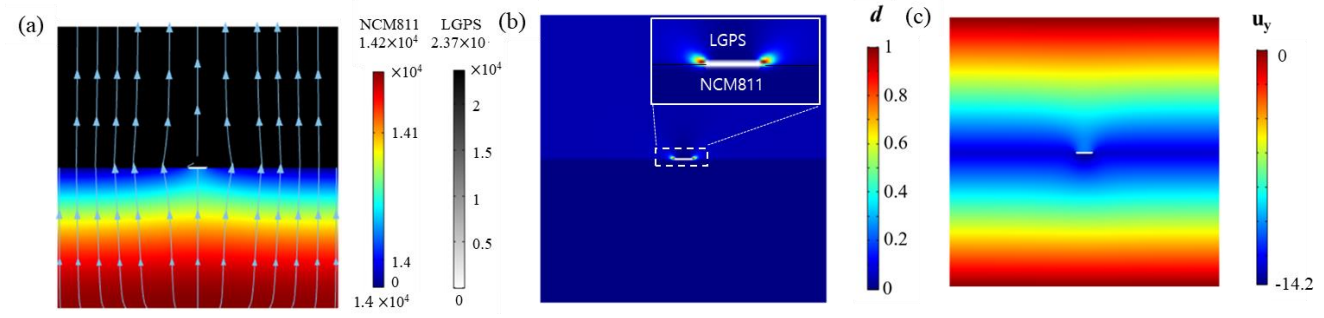

Fig. S2 Electro-chemo-mechanical responses of (a) Li concentration [mol/m^3], (b) crack field [*0*≤d≤1], (c) displacements [u_y(nm)] at 1620s (SOC=0.42).

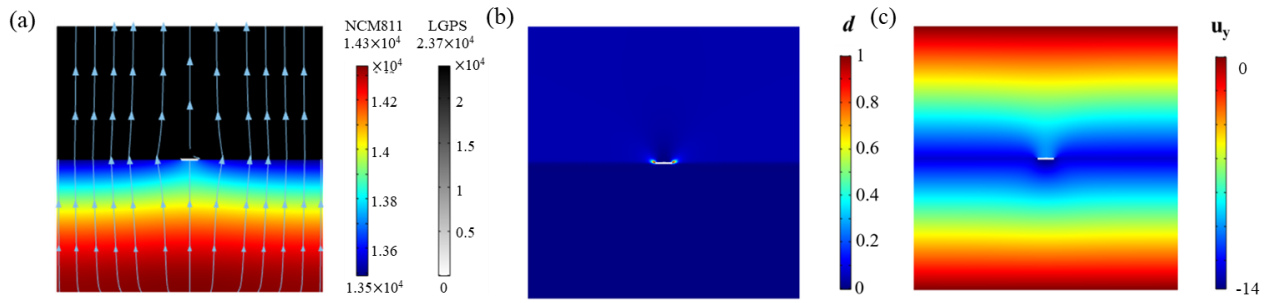

Fig. S3 Electro-chemo-mechanical responses of (a) Li concentration [mol/m^3], (b) crack field [*0*≤d≤1], (c) displacements [u_y(nm)] at the t=323s (SOC=0.43) to initiate the crack under 5 C-rate**.**

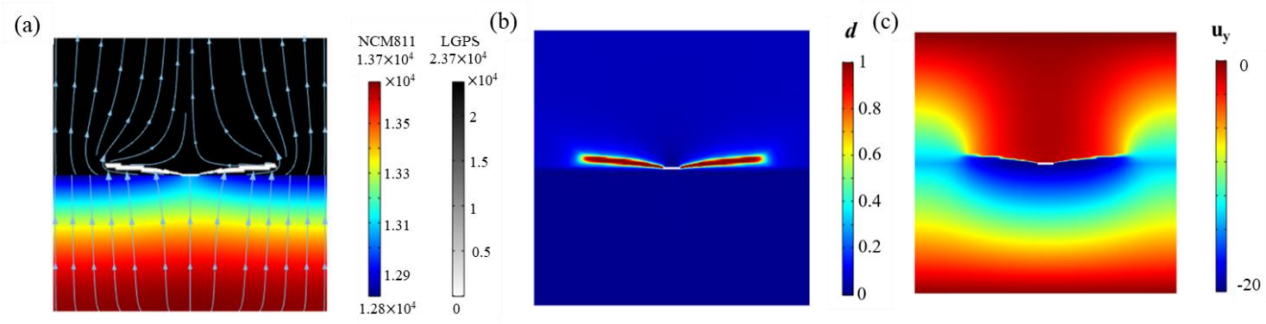

Fig. S4 Electro-chemo-mechanical responses of (a) Li concentration [mol/m^3], (b) crack field [*0*≤d≤1], (c) displacements [u_y(nm)] during the crack propagation under 5 C-rate.

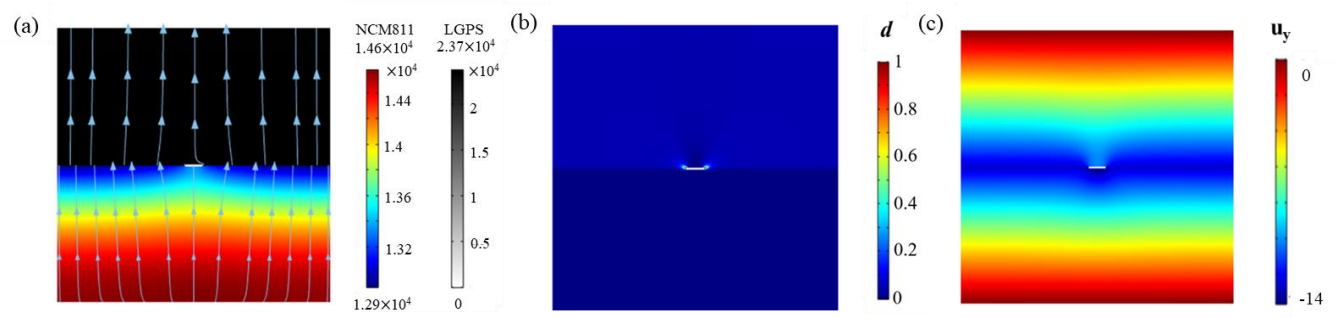

Fig. S5 Electro-chemo-mechanical responses of (a) Li concentration [mol/m^3], (b) crack field [*0*≤d≤1], (c) displacements [u_y(nm)] at the t=162s (SOC=0.46) to initiate the crack under 10 C-rate.

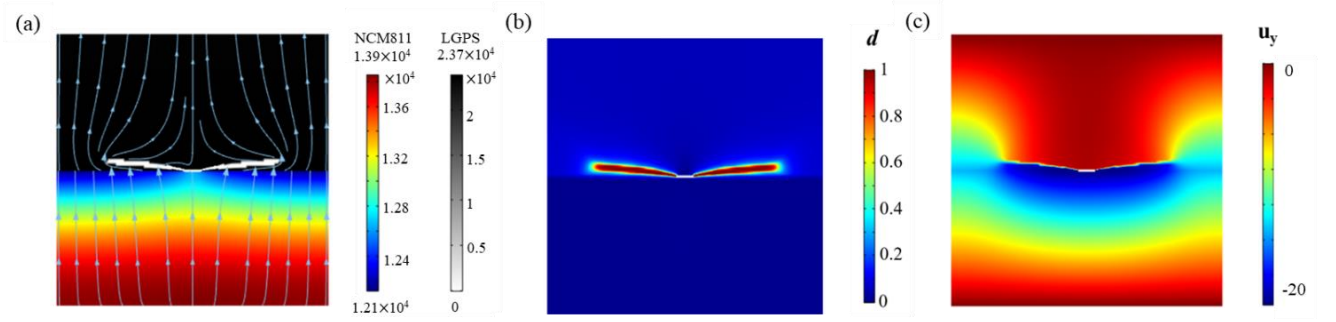

Fig. S6 Electro-chemo-mechanical responses of (a) Li concentration [mol/m^3], (b) crack field [*0*≤d≤1], (c) displacements [u_y(nm)] during the crack propagation under 10 C-rate.

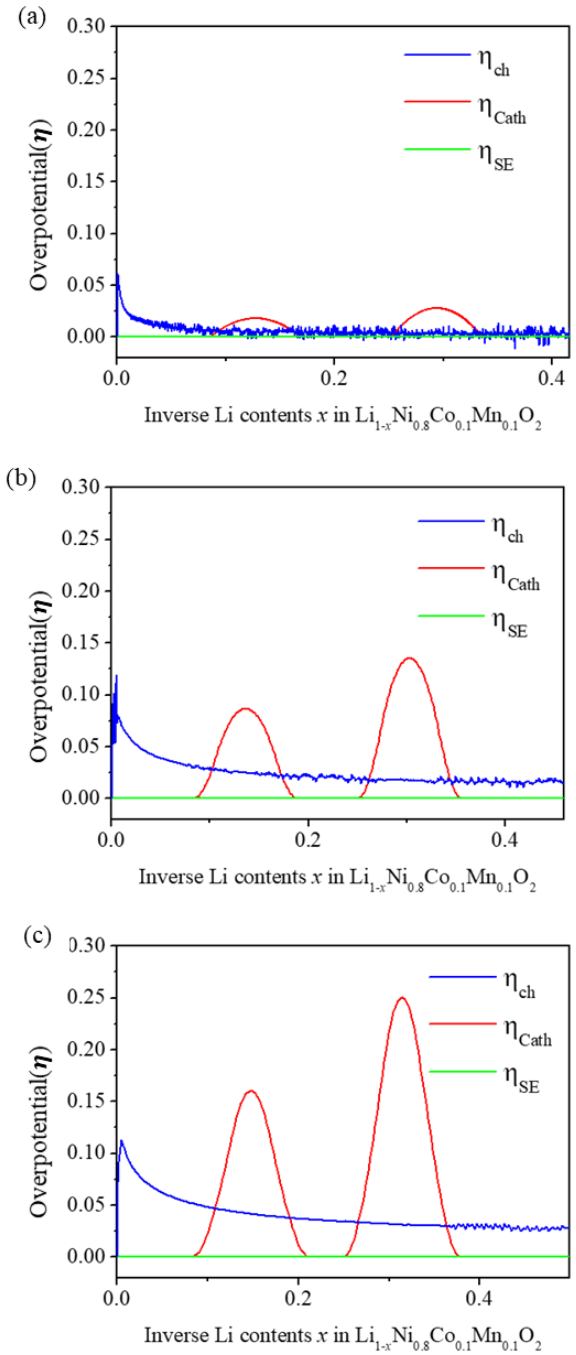

Fig. S7 Overpotential (***η***) as a function of Inverse Li contents *x* in $Li_{1-x}Ni_{0.8}Co_{0.1}Mn_{0.1}O_2$ depending on the different C-rates.(a, b and c are 1 , 5 and 10 C-rate respectively.)

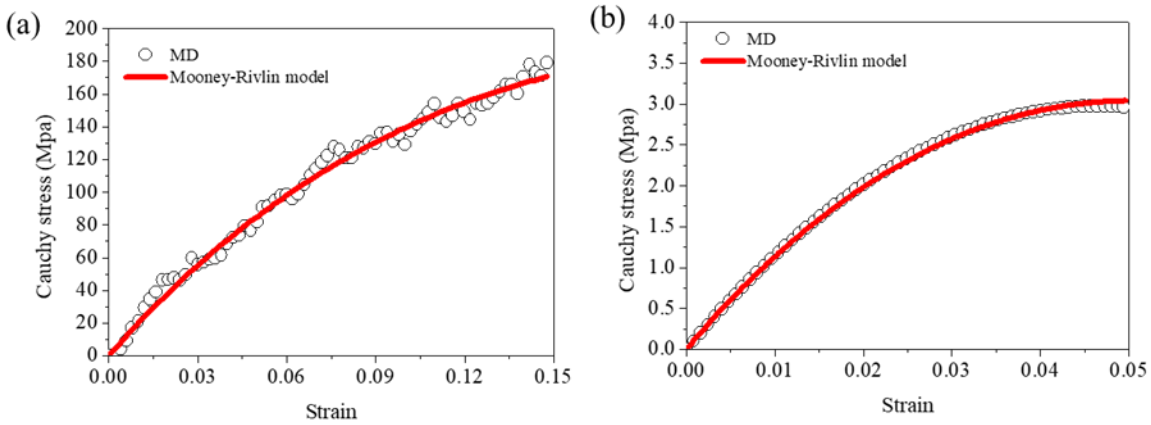

Fig. S8 Hyperelastic behaviors of (a) the polyamide and (b) the PDMS for the uniaxial tensile loading test based on MD simulation and Mooney-Rivlin model.

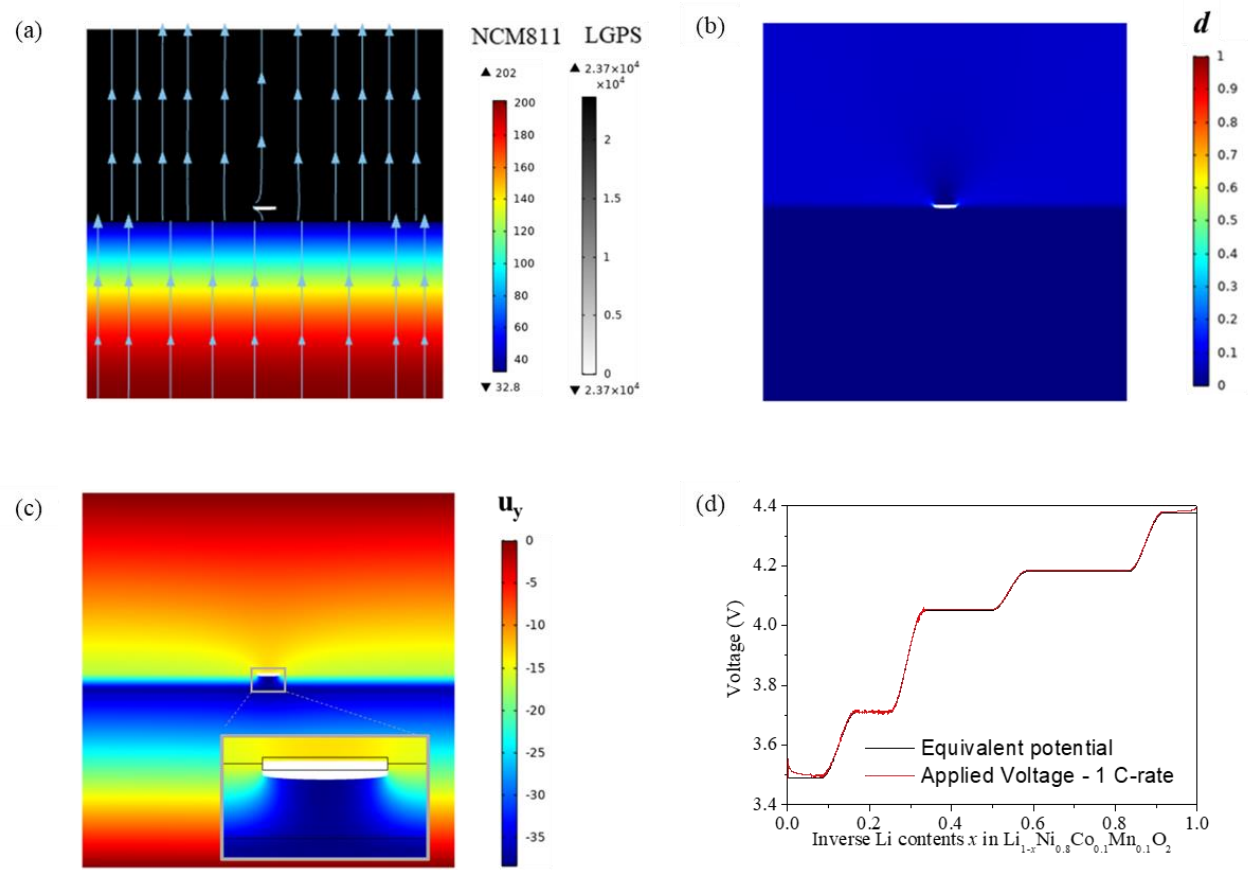

Fig S9 Electro-chemo-mechanical responses of (a) Li concentration[mol/m^3], (b) crack field [*0*≤d≤1], (c) displacements [nm] (inset is displacement fields near crack tip and black line is initial configuration) and (d) Voltage profiles [V] as a function of Inverse Li contents x in $Li_{1-x}Ni_{0.8}Co_{0.1}Mn_{0.1}O_2$,where red is the calculated operating voltage and black line is the equivalent potential, at fully discharged state for the multiscale model with the polyamide filler under $\frac{t_{filler}}{t_{NCM811}} = 0.075$ condition.

Table S1. Symbols of electrochemical equations

Notation	Description [Dimension]
Li^+	Lithium ion
e^-	Electron
I_{Anode}	Reaction current of Anode [A]
I^0_{Anode}	Exchange current of Anode [A]
$I_{Cathode}$	Reaction current of Cathode [A]
$I^0_{Cathode}$	Exchange current of Cathode [A]
J_k	Flux of species k [mol/(m^2s)]
D_k	Diffusion coefficient of species k [m^2/s]
c_k	Concentration of species k [mol/m^3]
α_k	Charge transfer coefficient for the reaction of electrode
k_d	Reaction rate constant Li ion generation
k_r	Reaction rate constant of Li ion recombination
η	Over potential [V]
V	Potential of electrode [V]
E_{eq}	Equilibrium potential [V]
F	Faraday's constant [96485 C/mol]
R	Gas constants [8.314 J/(mol K)]
T	Temperature [K]
L_1	Thickness of solid electrolyte [m]
L_2	Thickness of cathode [m]

Table S2. Mechanical elastic constants [Gpa], moduluses [Gpa] and Poisson's ratio for NCM811.

C_{11}	C_{12}	C_{13}	C_{33}	C_{44}	B	G	Y	v
163.9	103.4	22.1	219.9	51	93.7	53.1	134	0.26

Table S3. Mechanical elastic constants [Gpa], moduluses [Gpa] and Poisson's ratio for LGPS.

C_{11}	C_{12}	C_{13}	C_{33}	C_{44}	C_{66}	B	G	Y	v
41.6	22.89	11.65	43.1	9.5	14.7	24.3	12.8	31.1	0.29